


ORIGINAL ARTICLE

Open Access



# Bulging Distortion of Austenitic Stainless Steel Sheet on the Partially Penetrated Side of Non-Penetration Lap Laser Welding Joint

Chengwu Yao<sup>1\*</sup> , Enze Liu<sup>1</sup>, Jiaming Ni<sup>2</sup> and Binying Nie<sup>3</sup>

## Abstract

Non-penetration laser welding of lap joints in austenitic stainless steel sheets is commonly preferred in fields where the surface quality is of utmost importance. However, the application of non-penetration welded austenitic stainless steel parts is limited owing to the micro bulging distortion that occurs on the back surface of the partial penetration side. In this paper, non-penetration lap laser welding experiments, were conducted on galvanized and SUS304 austenitic stainless steel plates using a fiber laser, to investigate the mechanism of bulging distortion. A comparative experiment of DC01 galvanized steel-Q235 carbon steel lap laser welding was carried out, and the deflection and distortion profile of partially penetrated side of the sheets were measured using a non-contact laser interferometer. In addition, the cold-rolled SUS304 was subjected to heat holding at different temperatures and water quenching after bending to characterize its microstructure under tensile and compressive stress. The results show that, during the heating stage of the thermal cycle of laser lap welding, the partial penetration side of the SUS304 steel sheet generates compressive stress, which extrudes the material in the heat-affected zone to the outside of the back of the SUS304 steel sheet, thereby forming a bulge. The findings of these experiments can be of great value for controlling the distortion of the partial penetrated side of austenitic stainless steel sheet during laser non-penetration lap welding.

**Keywords** Non-penetration lap laser welding, Bulging distortion, Austenitic stainless steel, Compressive stress, Tension stress

## 1 Introduction

Austenitic stainless steel and galvanized steel sheet joints are commonly used in decorative structures, household kitchen utensils, buildings, elevators, and architectural trim panels. Furthermore, they have the advantages of

better appearance, corrosion resistance and cost effectiveness. In these application areas, even though the strength requirements for thin-plate joints are low, good appearance is extremely strict; and any defect on the surface of the austenitic stainless steel sheet, can reduce the consumer's subjective evaluation of the product. Gluing and various welding methods like non-penetration welding are commonly used for joining such sheets. Glued joints have various advantages over welding such as no distortion, and lower processing difficulty [1], but the disadvantages of glued joints are also serious. The glued joints are deteriorated with time, and joint failure can easily occur [2]. In contrast, the mechanical properties of non-penetration welded joints remain stable, and the surface integrity of the partially penetrated side of the

\*Correspondence:

Chengwu Yao  
yaochw@sjtu.edu.cn

<sup>1</sup> Shanghai Key Laboratory of Materials Laser Processing and Modification, School of Material Science and Engineering, Shanghai Jiao Tong University, Shanghai 200240, China

<sup>2</sup> Shanghai Aerospace Precision Machinery Institute, Shanghai 201600, China

<sup>3</sup> Chemical and Biological Engineering College, Yichun University, Yichun 336000, China



© The Author(s) 2024. **Open Access** This article is licensed under a Creative Commons Attribution 4.0 International License, which permits use, sharing, adaptation, distribution and reproduction in any medium or format, as long as you give appropriate credit to the original author(s) and the source, provide a link to the Creative Commons licence, and indicate if changes were made. The images or other third party material in this article are included in the article's Creative Commons licence, unless indicated otherwise in a credit line to the material. If material is not included in the article's Creative Commons licence and your intended use is not permitted by statutory regulation or exceeds the permitted use, you will need to obtain permission directly from the copyright holder. To view a copy of this licence, visit <http://creativecommons.org/licenses/by/4.0/>.

austenitic stainless steel can be guaranteed [3–5]. Laser welding energy is more concentrated than other welding methods, and its welding heat affected zone is smaller as well, which is more advantageous and widely used in thin plate lap welding [6, 7]. Therefore, non-penetration laser lap welding may be an alternative to gluing for such steel sheet lap joints with higher surface quality requirements [8–10]. However, in this type of welding, bulging distortion occurs on the non-penetration side of the austenitic stainless steel plate [11–14]. Even though this distortion is of micron scale, it seriously affects the surface quality of the welded joint. This is a serious problem and needs to be solved urgently.

Many researchers have done studies on various types of distortions occurring during the laser welding process of thin plates. Huang et al. [15] studied the welding deformation of thin plates based on the inherent strain theory, and considered that the deformation of butt welding of thin plate is generally produced by the longitudinal and transverse inherent strains. Matsuokaa et al. [16] studied the thermal distortion of thin stainless steel sheet in the bead-on-plate welding by using a single mode fiber laser with a Galvano scanning system, and concluded that the angle deformation of thin stainless steel sheet in laser micro-welding was due to both the shrinkage of width direction related to humping and the expansion of weld bead with the convex curvature on the top surface. Choobi et al. [17] considered the laser welding deformation of thin plates is mainly angular deformation, and used a self-built artificial neural network model to reproduce the angular deformation that occurred during the welding of SUS304 stainless steel sheets. Liu [18] studied the non-penetration lap laser welding of SUS301 stainless steel plates of thickness 0.8 mm and 1.2 mm, and concluded that the deformation of SUS301 stainless steel plate on the partially penetrated side is an angular deformation mechanism. So far, the researches on laser welding distortion of thin plates mainly focused on large-scale macroscopic deformations, such as angular deformation, and its deformation characteristics are similar to those of traditional arc welding lap welding of thin plates [19]. However, there are few studies on the micro-scale deformation of thin plates. In reality, based on micro-scale analysis, it is found that the geometric shape and microstructure characteristics of the deformation zone of this welding mark are completely different from large-scale macroscopic deformations, and the deformation mechanism is also completely different [20, 21]. Therefore, the deformation mechanism studied on the macro-scale may sometimes be wrong conclusions. The engineers of some elevator panel manufacturing companies used the method of correcting the angular deformation to eliminate the bulging distortion of the partially penetrated

side of austenitic stainless steel sheet, but it had almost no effect, so non-penetration lap laser welding method has not used in the manufacture of elevator panels.

In this paper, the influence of laser power on the bulging distortion degree of the partially penetrated side of the lap welded joint of DC01 galvanized steel and SUS304 stainless steel sheet was studied, and it was compared with the lap joint of DC01 galvanized steel and Q235 carbon steel sheet. In addition, by characterizing the microstructure of the cold-rolled SUS304 stainless steel sheet after heat holding at 300–1000 °C, bending and water quenching, and comparing it with the microstructure of the bulging distortion zone of the SUS304 stainless steel sheet, the welding thermal cycle peak temperature and stress type of the bulging distortion zone in the partially penetrated side of SUS304 stainless steel sheet were obtained. Based on the above experiments, the distortion mechanism of the bulging distortion which occurred on the partially penetrated side of the SUS304 austenitic stainless steel sheet was discussed. These results can be very valuable for successful applications of non-penetration laser lap welding to austenitic stainless steel sheet components with high appearance quality requirements.

## 2 Materials and Methods

DC01 galvanized steel sheet and SUS304 austenitic stainless steel sheet each of size 110×110 mm, were used in the non-penetration lap laser welding experiments. The thickness of both DC01 galvanized and the SUS304 stainless steel sheets are 1.2 mm, and the SUS304 stainless steel sheet is the lower plate of the lap joint, which is in a cold-rolled state. The cold-rolled Q235 carbon steel sheet of the same size was also used, for the non-penetration lap laser welding joint of DC01 galvanized steel-Q235 carbon steel sheet. The chemical compositions of the test steel sheets used, are shown in Table 1, therein the thickness of the zinc layer of DC01 steel is 2.5 μm.

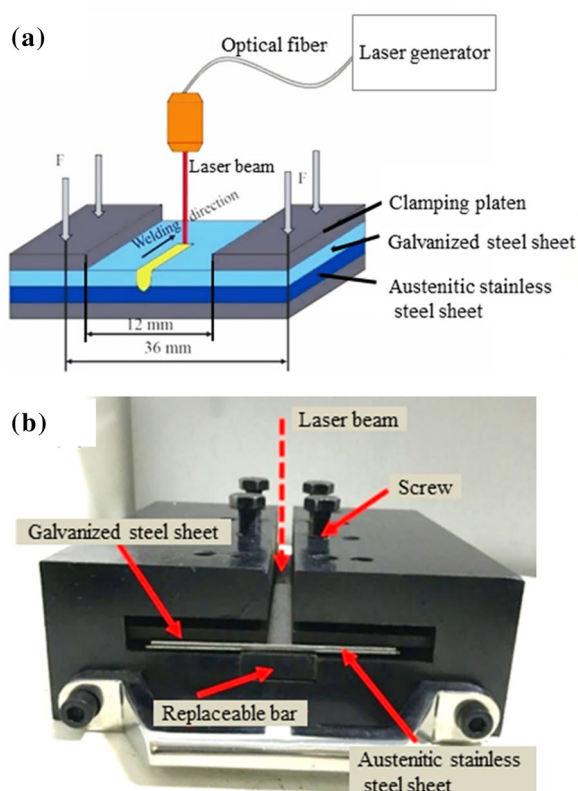
The YLS-10000 fiber laser produced by American IPG Company was used in the experiment. Zero defocus welding was adapted with the Gaussian beam diameter at the focus being 0.72 mm and the wavelength of  $\lambda = 1070\text{--}1080$  nm. The welding speed is controlled by Japanese FANUC robot. Pure laser welding was used for lap welding. The laser power is 1.9–2.6 kW, and the welding speed is 70 mm/s.

Figure 1(a) is a schematic of non-penetration laser welding system. Figure 1(b) is the photo of the welding fixture. The two sheets to be welded are stacked in a jig groove, the upper one is the DC01 galvanized steel sheet, and the lower one is the SUS304 stainless steel sheet.

Two pressure plates are respectively pressed on the two sides of the test sheets to be welded, and the bolts are screwed onto the pressure plate through bolt holes. The

**Table 1** Chemical compositions of SUS304 steel, DC01 steel, and Q235 steel

Plates	Elements (wt. %)							
	C	Mn	P	S	Si	Cr	Ni	Al
SUS304	0.027	1.6	0.01	0.002	0.36	18.5	11.6	–
DC01	0.1	0.5	0.035	0.025	–	–	–	0.02
Q235	0.14	0.55	0.025	0.008	0.19	–	–	–

**Figure 1** Schematic diagram and photo of welding fixture of non-penetration lap laser welding experiment

digital display detection torque wrench is used to tighten the bolts. In order to ensure that the clamp force of the sheet stack for each welding experiment is the same, the tightening torque of each bolt is set to 550 N·m. During laser welding, the laser illuminates the surface of the sheets in the middle groove region of the clamp, and the penetration depth of the SUS304 stainless steel sheet is controlled by adjusting the laser welding process parameters, to form a partially penetrated welded joint.

Due to the too small size of the bulging formation zone on the back surface of partially penetrated side of SUS304 stainless steel sheet, it is difficult to accurately measure the peak temperature of this zone during lap laser welding. Therefore, an experimental simulation method was

used to obtain the peak temperature of the welding thermal cycle of the bulging formation zone. The cold-rolled SUS304 stainless steel was heated to 300 °C, 400 °C, 500 °C, 600 °C, 700 °C, 800 °C, 900 °C, 1000 °C, respectively, and quenched immediately after 5 minutes of heat preservation. The microstructure of SUS304 stainless steel sheets after heating at different heat treatment temperatures was characterized. By comparing it with that the microstructure of the bulging distortion zone of partially penetrated side of SUS304 non-penetration welded joint, the peak temperature of the welding thermal cycle of the bulging distortion zone during lap laser welding was obtained. The cold-rolled SUS304 stainless steel sheet was heated at this peak temperature, bent and quenched, and the microstructure of the bent sheets under compressive stress of the interior arc and the tensile stress of the exterior arc were obtained. By comparing it with the microstructure of lap laser welded joint, the type of stress generated in bulging distortion zone was obtained.

The cross-sections of non-penetration lap welding joints of DC01 galvanized steel-SUS304 stainless steel, and DC01 galvanized steel-Q235 carbon steel, along with SUS304 stainless steel heat treated samples, were etched by aqua regia after grinding and polishing. The microstructures of the welded joints were observed by MCK-50MC metallographic microscope produced by Zeiss, and an electron scanning microscope of NOVA NanoSEM 230 produced by FEI. The ZeGage 3D surface profiler manufactured by ZYGO Co., Ltd., was used to measure the micro bulging distortion on the surface of the non-melting side of the austenitic steel sheet.

### 3 Results and Discussion

Figure 2 shows the macro morphologies of non-penetration lap welded joints of DC01-SUS304 and DC01-Q235 steel sheets, with welding speed of 70 mm/s and laser power of 2.0 kW. The weld is well formed without any obvious macro defects. It must be pointed out that, even if the penetration depth of the lap weld is only about 0.1 mm, a steep peak is still formed on the back of the partially penetrated side of lap welded joints of DC01-SUS304 steel sheets, with a peak height of about 6 μm, as shown by the red arrow in Figure 2(a). On the contrary, the bulging distortion of partially penetrated

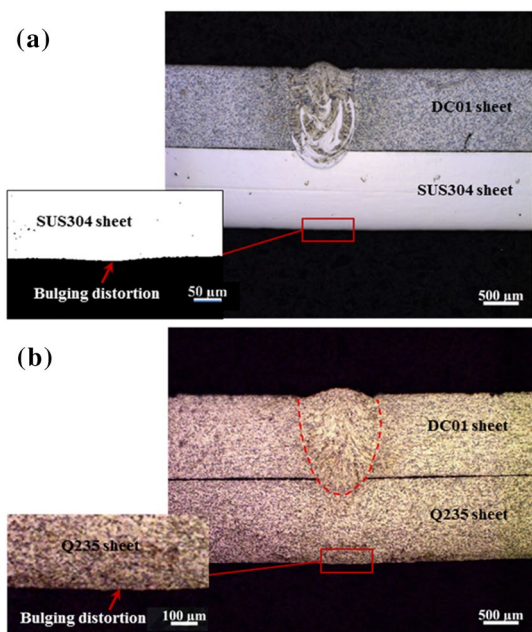


**Figure 2** Cross-section of lap laser welded joint: (a) DC01 galvanized steel and SUS304 austenite stainless steel sheet, (b) DC01 galvanized steel and Q235 carbon steel sheet

side of lap welded joints of DC01-Q235 steel sheets is gentle, as shown by the arrow in Figure 2(b), and there is a flat peak on the partially penetrated side, with a peak height of about 3 μm.

3D model of the bulging profile on the partially penetrated side of lap welded joint of DC01 galvanized steel-SUS304 steel sheets, as obtained by the profilometer is shown in Figure 3, in which different colors represent the relative height of different positions. Figure 3(a) shows a bulging profile model with the profilometer scanning width of 8 mm and laser power of 2.4 kW. It can be seen from Figure 3(a) that the distortion exhibits obvious angular deformation, but the bulging profile is mainly in the range of 2 mm in width. From the visual inspection of decorative parts, visual distortion will reduce the subjective evaluation of the surface quality of the material. Generally, steep peaks will cause large height fluctuations on the surface of the parts, which will change the reflection path of the incident light and cause visual distortion. Therefore, the visually distorted area on the partially penetrated side of the SUS304 steel sheet should also be the bulging distortion zone within a width of 2 mm. In view of this, the following research focuses on this 2 mm bulging distortion zone. Figure 3(b), (c), and (d) show the bulging profile models on the partially penetrated side of lap welded joints with a welding speed of 70 mm/s, and a laser power of 0 kW, 2.0 kW, and 2.6 kW, respectively. In the range of

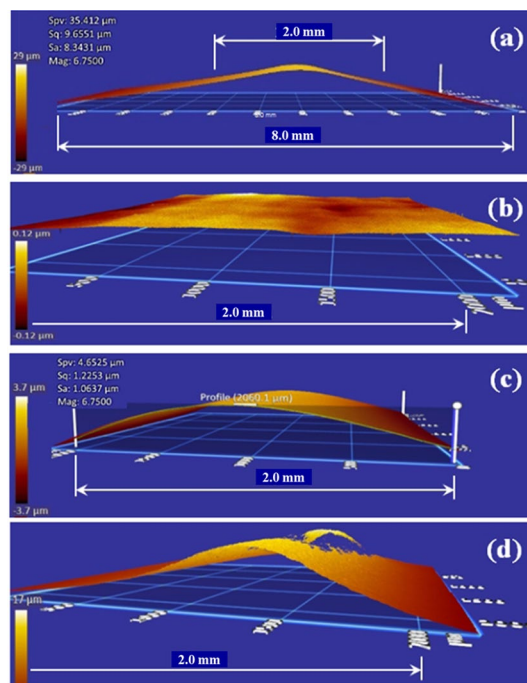


**Figure 3** 3D contour model of the bulging distortion of the lap SUS304 welded joint with different laser power: (a) 2.4 kW, the 8 mm scanning width, (b) 0 kW, 2 mm scanning width, (c) 2.0 kW, 2.0 mm scanning width, (d) 2.6 kW, 2.0 mm scanning width

2 mm in width, the maximum peak heights are 0 μm, 6 μm, and 27 μm, respectively.

In order to describe the bulging distortion more directly, the position data of the 3D model of the bulging profile was derived from the profilometer, and the 2D profile of the bulging distortion in the vertical welding direction was drawn based on these data, as shown in Figure 4. The profile of the bulging distortion zone of the lap welded joint of galvanized steel-SUS304 stainless steel sheets is shown in Figure 4(a). The region with the most obvious distortion, between two dotted lines, is at the center of the weld, and its width is about 2 mm. The profile of the bulging distortion is substantially a bilaterally symmetrical curve. When the laser power is lower than 2.0 kW, the curve is gentle, and the radius of curvature at the peak is large, and the slope of each point in the curve remains stable, indicating that the bulging distortion has the characteristic of angular distortion. As the laser power increases, the curve becomes steeper, the radius of curvature at the peak gradually decrease. When the laser power is increased to 2.2 kW or higher, the slope of the curve increases sharply, and the angular deformation feature of the bulging distortion zone disappears. Figure 4(b) shows the outline curve of the bulging distortion zone of the lap welded joint of galvanized steel-Q235 steel sheets.

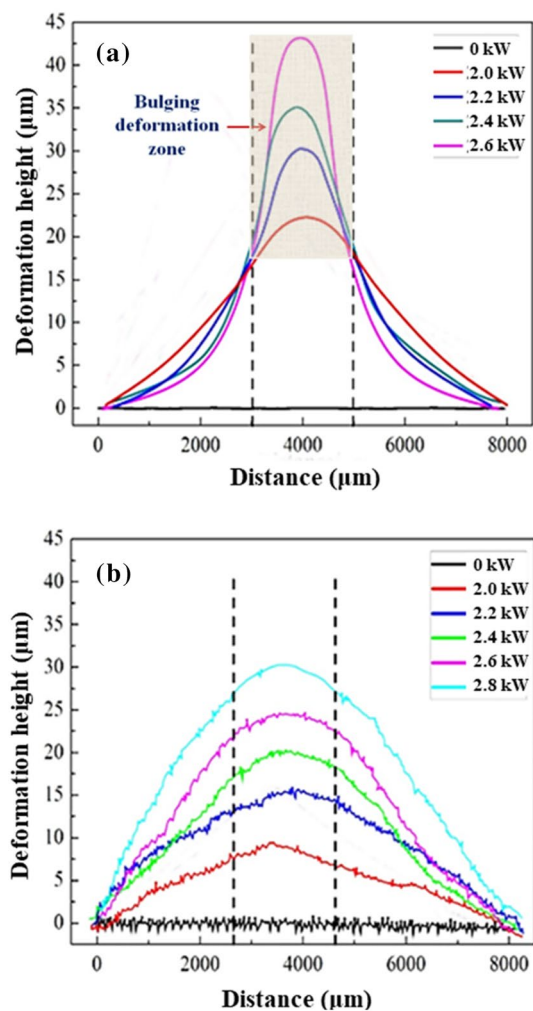


**Figure 4** Outline curves of the deformation of the lap laser welded joints at different laser welding power: (a) DC01-SUS304 steel plates, (b) DC01-Q235 steel plates

When the laser power is 2.0 to 2.8 kW, the partially penetrated side of Q235 steel sheet, does not show the sharp bulging distortion similar to that of SUS304 stainless steel sheet, but shows the feature of angular deformation.

By comparing Figure 4(a) and (b), it is found that the peak of the curve of the bulging distortion zone of Q235 steel sheet is lower than that of SUS304 steel sheet, and the slope of the curve is also lower than that of SUS304 steel sheet. For example, the lap laser power is 2.6 kW, the peak height of the contour curve of the bulging distortion zone of Q235 steel sheet is about 5  $\mu\text{m}$ , and the slope is about 0.005, while the peak height of the curve of SUS304 steel sheet is about 27  $\mu\text{m}$ , and the slope is about 0.024. Since the slope of the curve of the deformation zone of the Q235 carbon steel sheet is small, it has less influence on the reflected light, which will not cause

visual distortion and deteriorate the surface quality of Q235 steel sheet.

Figure 5 shows the macroscopic morphology and microstructure of the SUS304 sheet on the partially penetrated side of the lap welded joint of DC01 galvanized steel-SUS304 stainless steel sheets. Figure 5(a) shows the morphology of the partially penetrated side of the lap welded joint. The welding heat-affected zone of the SUS304 steel sheet is in the shape of "V". Figure 5(b) shows the overheated zone near the fusion line, where the elongated original grains in the cold-rolled state, are completely recrystallized into coarse equiaxed grains. As shown in Figure 5(c), in the heat affected zone far from the fusion line, the recrystallized equiaxed grains become finer. Figure 5(d) shows, that even in the edge of the SUS304 stainless steel sheet, the original cold-rolled grains still disappear, and the elongated grains almost completely recrystallized into equiaxed grains. Figure 5(e) shows the EBSD image of the bulging distortion zone of the back surface of the SUS304 steel sheet, as shown by the arrow, there are a large number of sub-grains in the equiaxed grains, indicating that stress plastic distortion is accompanied by the formation of equiaxed grains.

Twins were observed in these equiaxed grains in the heat-affected zone of the SUS304 steel sheet, and the twins generated at different positions have different morphologies. As shown in Figure 5(b) and (c), these regions have higher temperatures due to being closer to the fusion line, resulting in coarser recrystallized equiaxed grains, and twins are also coarse and traverse the entire grains, which are typical annealing twins. The bulging distortion zone is located at the edge of SUS304 steel sheet, which has fine recrystallized equiaxed grains because it is far from the fusion line, as shown in Figure 5(d). A large number of densely-concentrated clusters of fine twins appear in the equiaxed grains, as shown by the red arrows, and the twin planes of these twins tend to be perpendicular to the cold rolling direction of the SUS304 steel sheet. These twins are lenticular, originate from the grain boundaries and end in the interior of the grains, which are typical deformation twins.

Figure 6 shows the water-quenched microstructure of the cold-rolled SUS304 steel sheet held at 300  $^{\circ}\text{C}$  to 700  $^{\circ}\text{C}$  for 5 min. After being held at 300  $^{\circ}\text{C}$  to 700  $^{\circ}\text{C}$  for 5 min, the cold-rolled SUS304 sheet was in the recovery stage, and its grain morphology was still in the form of fibers elongated in the rolling direction, as shown in Figure 6(a)–(e). After being held at 800  $^{\circ}\text{C}$  for 5 min, a small amount of annealed twins appeared in the cold-rolled SUS304 sheet, as shown in Figure 6(f). After being held at 900  $^{\circ}\text{C}$  for 5 min, a small amount of recrystallized equiaxed grains appeared, as shown in Figure 6(g). After

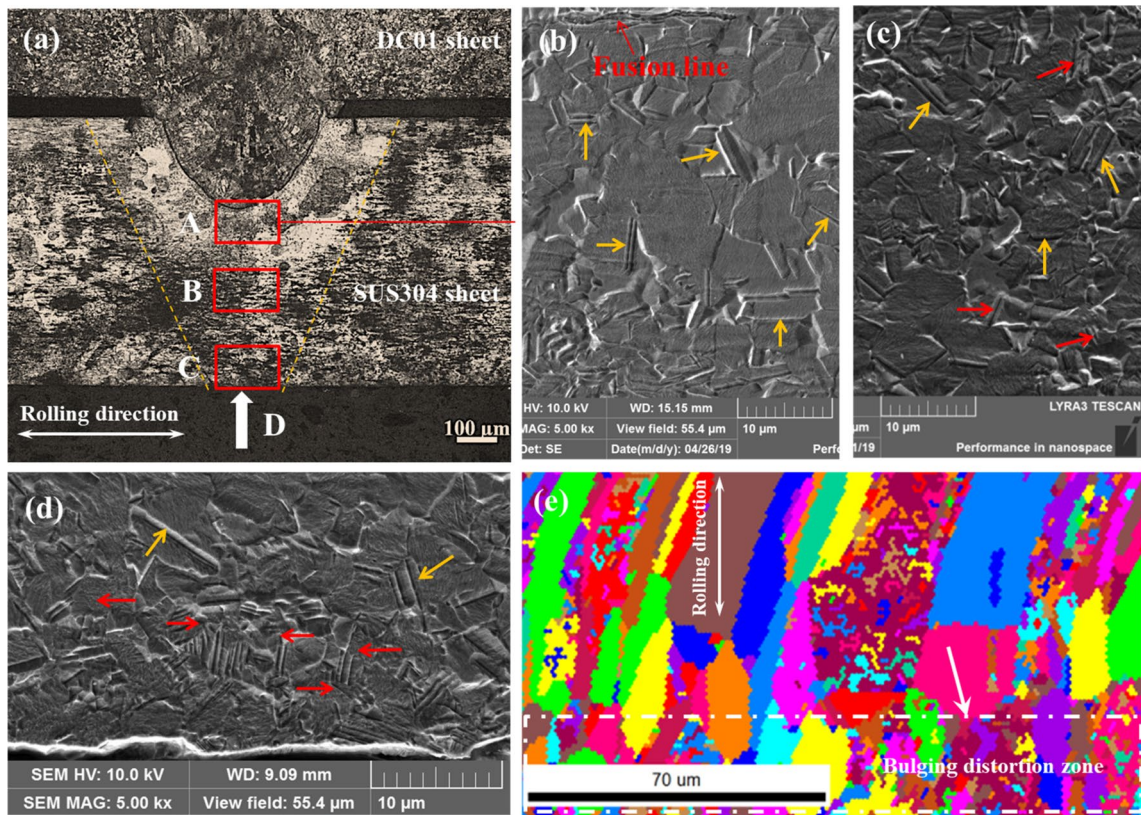


**Figure 5** Cross-section morphology of the lap welded joint of the SUS304 steel sheet: (a) Lap welded joint, (b) SEM microstructure at the “A” mark in (a), (c) SEM microstructure at the “B” mark in (a), (d) SEM microstructure at the “C” mark in (a), (e) EBSD grain map of the backsurface of the SUS304 sheet, at the “D” mark in (a)

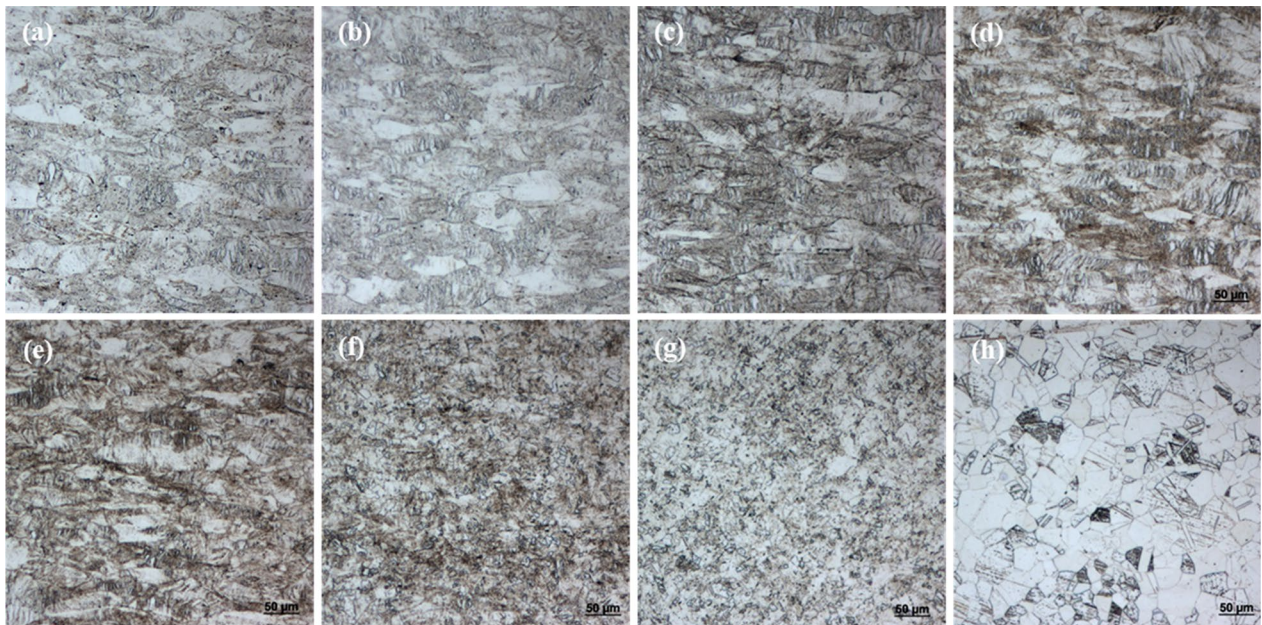


**Figure 6** Microstructure of cold-rolled SUS304 stainless steel sheet heated at different temperatures: (a) 300 °C, (b) 400 °C, (c) 500 °C, (d) 600 °C, (e) 700 °C, (f) 800 °C, (g) 900 °C, (h) 1000 °C (The original cold rolled grains have been completely recrystallized into equiaxed grains)

being held at 1000 °C for 5 min, as shown in Figure 6(h), a large number of the recrystallized equiaxed grains and annealing twins appeared in the cold-rolled SUS304 steel sheet, which was similar to the microstructure of the welding heat-affected zone of the SUS304 steel sheet, as shown in Figure 5. Therefore, the effect of heat treat at 1000 °C for 5 min on the microstructure of the cold-rolled SUS304 steel sheet was similar to that of the peak temperature of the thermal cycle of lap laser welding on the microstructure of the bulging distortion zone.

In order to analyze the type of stress that caused the deformation twins to be generated in the bulging distortion zone of the non-penetration lap welded joint, the cold-rolled SUS304 steel sheet was held at 1000 °C for 5 min, and then immediately bent and quenched. Figure 7(a) shows the macroscopic shape of the bent cold-rolled SUS304 steel sheet.

According to the stress distribution theory of plane bending structure [22–24], the outer arc of the bent SUS304 sheet is subjected to tensile stress  $\sigma_T$ , and the

inner arc is subjected to compressive stress  $\sigma_C$ . Figure 7(b) shows the optical micrograph of the inner arc of the bent SUS304 sheet, where the recrystallized equiaxed grains are compressive into flat grains by compressive stress. Due to the preferential twins caused by compressive stress, the twin plane of annealed twins tends to be perpendicular to the compressive stress, that is, perpendicular to the rolling direction of the cold-rolled SUS304 sheet, as shown by the light blue arrows. In addition, the dense deformation twins occur in the inner arc of the bent sheet, as shown in Figure 7(c), and their direction is also perpendicular to the rolling direction of the cold-rolled SUS304 sheet. The recrystallized grains in the outer arc of the bent SUS304 sheet are elongated by tensile stress, as shown in Figure 7(d). The twin plane of annealed twins tends to be parallel to the tensile stress, that is, parallel to the rolling direction of the cold-rolled SUS304 sheet, as shown in Figure 7(e). Due to the absence of stress, the recrystallized equiaxed grains in the center of the bent SUS304 sheet still retain the polygonal

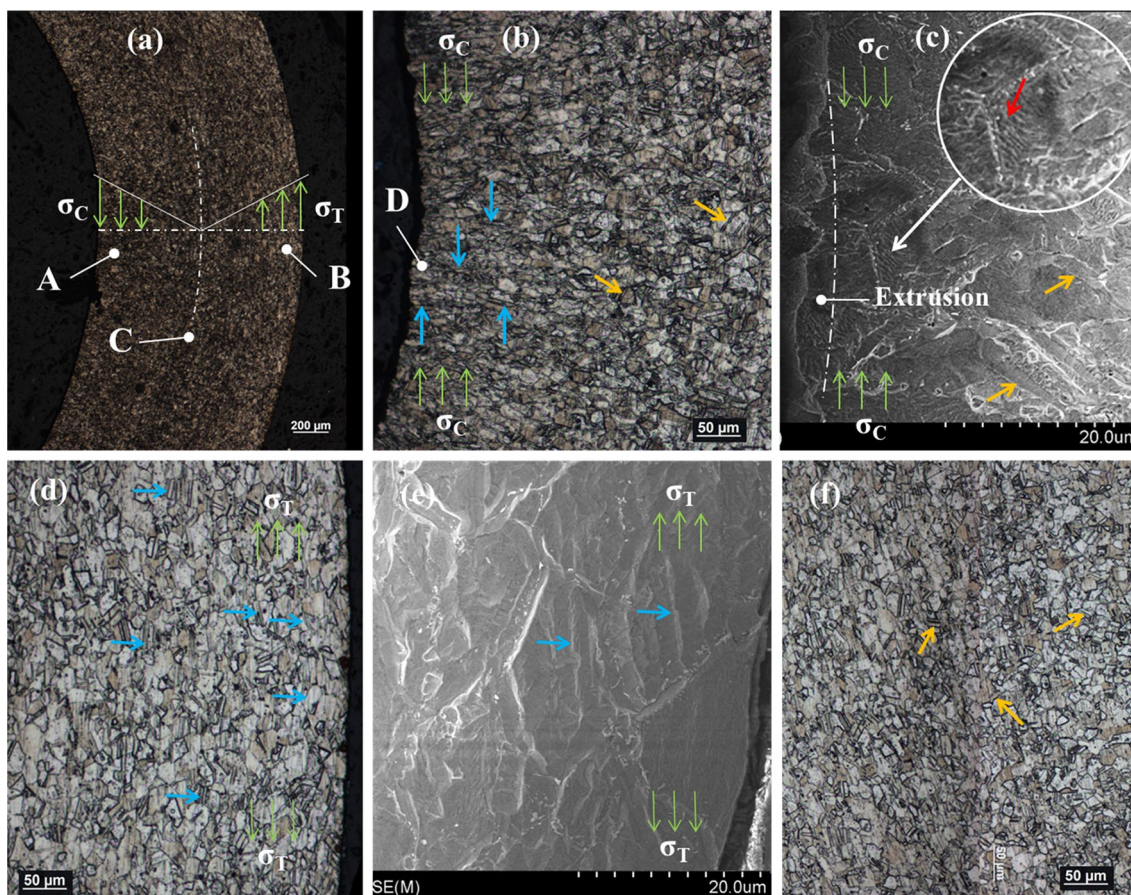


**Figure 7** Cross-section of SUS304 stainless steel sheet after heating, bending, and water quenching: (a) Cross-section of the bent sheet, (b) Optical micrograph at “A” mark in (a), (c) SEM micrograph at “D” mark in (b), (d) Optical micrograph at “B” mark in (a), (e) SEM micrograph at the “B” mark in (a), (f) Optical micrograph at the “C” mark in (a)

shape, and the twin planes of the annealed twins have no obvious directionality, as shown by the yellow arrow in the Figure 7(f).

Comparing Figures 5 and 7, the deformation twins formed in the bulging distortion zone of the SUS304 steel sheet of the lap welded joint are similar to the deformation twins formed in the inner arc of the bent SUS304 sheet. Therefore, it can be inferred that the type of stress that caused the bulging distortion of the partially penetrated side of SUS304 steel sheet is the same as the type of the stress in the inner arc of the bent SUS304 sheet, that is, compressive stress. However, non-penetration lap laser welding of thin plates did not always lead to steep bulging distortion. As shown in Figure 4(b), the curve of the distortion zone of the lap welded joint of the DC01 galvanized steel-Q235 carbon steel sheet was a flat slope, which may be due to the lower compressive stress on the partially penetrated side of the Q235 steel sheet.

In this research, the SUS304 and Q235 sheets are clamped by the rigid support of the clamp, with an opening for laser welding, as shown in Figure 1, there is rigid restraint in the width direction of the non-penetration lap welded joints. During the laser welding process, the heat-affected zone (the "V" shaped area shown in Figure 5(a) on the partially penetrated side thermally

expands, and due to the constraint from the lower temperature materials on both sides of this zone, compressive stress is generated. The thermal expansion coefficient of SUS304 stainless steel is  $18.4 \times 10^{-6}/^{\circ}\text{C}$ , which is about 167% of that of Q235 steel ( $11 \times 10^{-6}/^{\circ}\text{C}$ ) at the same temperature. The thermal conductivity of SUS304 stainless steel is  $12 \text{ W}\cdot\text{m}^{-1}\cdot\text{K}^{-1}$ , which is only about 23% of that of Q235 steel ( $51 \text{ W}\cdot\text{m}^{-1}\cdot\text{K}^{-1}$ ) [25–29]. Therefore, the thermal expansion of the SUS304 sheet in the heat-affected zone is much higher than that of Q235 carbon steel, which causes the compressive stress generated on the partially penetrated side of the SUS304 sheet to be greater than that of the Q235 sheet. Due to the small thickness of the sheet, the heat-affected zone can easily extend to the back side of the partially penetrated side of lap welded joint. Comparing Figures 5(d) and 6(g), the instantaneous temperature of the welding thermal cycle in the bulging distortion zone of the SUS304 sheet is above  $900^{\circ}\text{C}$ , which causes the tensile strength of the SUS304 sheet to drop sharply below 90 MPa [30, 31]. Therefore, even if the compressive stress is low, the material in the heat-affected zone of SUS304 sheet will be plastically deformed.

According to the above analysis, the deformation mechanism of the bulging distortion on the

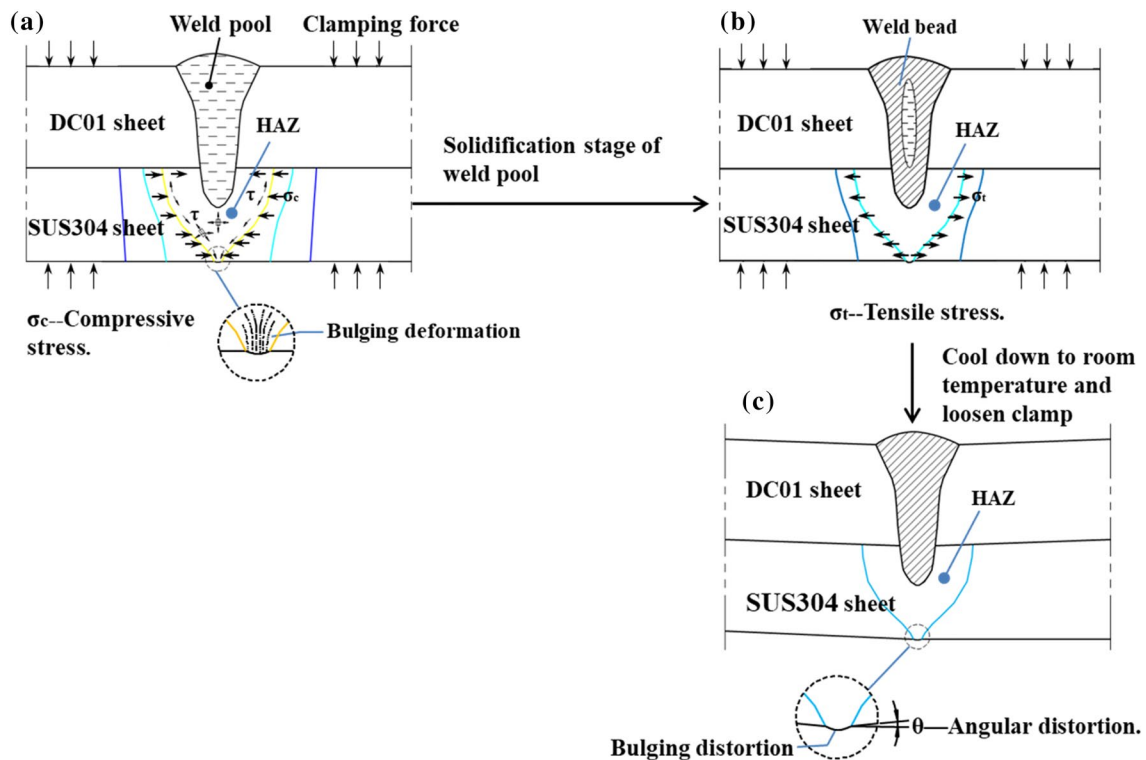


**Figure 8** Schematic diagram of the bulging distortion: (a) Formation stage of weld pool, (b) Solidification stage of weld pool, (c) Cool down to room temperature and loosen clamp



non-penetration side of austenitic stainless steel sheet, can be described as follows: as shown in Figure 8(a), the expansion of the "V"-shaped heat-affected zone on the partially penetrated side of the SUS304 sheet, is constrained by the adjacent low temperature zone and the rigid of the clamp on the overlapped steel sheets, and generates compressive stress. Consequently, the metal in the heat-affected zone ("V" shaped HAZ) is "extruded" by the compressive stress. Due to the high welding thermal cycle temperature, the strength of the SUS304 austenitic stainless steel sheet on the partially penetrated side of the lap welded joint is lower than the compressive stress, which causes the metal in the heat-affected zone of the SUS304 sheet to be extruded out of the back plane, thereby forming the bulging distortion. Since the extrusion deformation is formed in the tiny area of the heat-affected zone on the back of the SUS304 sheet, the peak of the bulging distortion forms is steep. As the temperature decreases, the weld pool solidifies and shrinks gradually, which causes the transition from the compressive stress to the tensile stress in the "V" shaped HAZ, as shown in Figure 8(b). After the lap welded joint is cooled to room temperature and the clamps are released, the tensile stress causes the angular deformation of SUS304 stainless steel sheet, as shown in Figure 8(c), while the bulging distortion is still retained.

#### 4 Conclusions

According to the research in this paper, the Q235 carbon steel sheet on partially penetrated side of laser lap welded joint only shows angular deformation, while the SUS304 austenitic stainless steel sheet shows steep bulging distortion. SUS304 austenitic steel has higher thermal expansion coefficient and lower thermal conductivity than Q235 carbon steel, so higher compressive stress is generated on the partially penetrated side of the SUS304 steel sheet of the lap welded joint, which causes the metal in the heat-affected zone to be extruded out of the back plane of the SUS304 sheet, thereby forming the bulging distortion. The bulging distortion of the SUS304 sheet is formed in the heating stage of the laser welding thermal cycle, which is different from the angular deformation of the Q235 plate formed in the cooling stage of the welding thermal cycle. Therefore, in the practical engineering application of non-penetration lap laser welding, it is difficult to reduce the bulging distortion of the partially penetrated side of the austenitic stainless steel sheet to improve its surface quality by adopting measures to control angular deformation. Since the bulging distortion is formed in the tiny area of the heat-affected zone of austenitic stainless steel sheet, the effective measures may

be to cut the peak of the compressive stress in the heat-affected zone by applying tensile stress.

#### Acknowledgements

The authors sincerely thank Hitachi (China) Research & Development Corporation for their help with the welding process.

#### Authors' Contributions

CY conceived ideas, methodology, performed microstructural; EL conducted experiments, prepared the analysis of microstructure, prepared manuscript; JN carried out one part of microstructural analysis; BN revised the manuscript. All authors read and approved the final manuscript.

#### Authors' information

Chengwu Yao, born in 1973, is currently a teacher at School of Material Science and Engineering, Shanghai Jiao Tong University, China. He received his doctor degree from Shanghai Jiao Tong University, China, in 2010. His research interests include welding and additive manufacturing. Tel: +86-21-34203024; E-mail: yaochwu@sjtu.edu.cn.

Enze Liu, born in 1994. He received his master degree on materials science and engineering from Shanghai Jiao Tong University, China, in 2020. E-mail: lezsz@qq.com

Jiaming Ni, born in 1983, is currently a senior engineer at Shanghai Aerospace Precision Machinery Institute, China. He received his doctor degree from Shanghai Jiao Tong University, China, in 2012. His research interests include laser welding. E-mail:weldspace@163.com.

Binying Nie, born in 1969, is currently a teacher at Chemical and Biological Engineering College, Yichun University, China. She received her master degree from Nanchang University, China, in 2008. E-mail: nby9697@126.com.

#### Funding

Not applicable.

#### Data availability

All relevant data are within the paper.

#### Declarations

#### Competing Interests

The authors declare no competing financial interests.

Received: 29 April 2021 Revised: 9 August 2022 Accepted: 21 December 2023

Published online: 16 January 2024

#### References

- [1] N Ratsch, S Böhm, M Voß, et al. Accelerated curing of glued-in threaded rods by means of inductive heating - Part I: experiments. *The Journal of Adhesion*, 2021, 97(1/4): 225–250.
- [2] H Q Ma, Q N Wang, L Qian, et al. Damage mode and failure mechanism of cementing structure. *Failure Analysis and Prevention*, 2012, 7(3): 162–166.
- [3] H Z Wang, M Nakanishi, Y Kawahito. Effects of welding speed on absorption rate in partial and full penetration welding of stainless steel with high brightness and high power laser. *Journal of Materials Processing Technology*, 2017, 249: 193–201.
- [4] P F Bai, Z J Wang, S S Hu, et al. Sensing of the weld penetration at the beginning of pulsed gas metal arc welding. *Journal of Manufacturing Processes*, 2017, 28(1): 343–350.
- [5] H Liang, Y Kan, Y L Jiang, et al. Mechanical properties of laser overlap welded joints of stainless steel sheets. *Chinese Journal of Lasers*, 2018, 45(6): 48–55. (in Chinese)
- [6] Z L Xue, J Q Shen, S S Hu. Influence of scanning speed and defocus distance on laser welded PA6GF30/SUS444 dissimilar lap joints. *Optics & Laser Technology*, 2022, 153: 108223

- [7] P Liu, KY Feng, G M Zhang. A novel study on laser lap welding of refractory alloy 50Mo–50Re of small-scale thin sheet. *Vacuum*, 2017, 136: 10–13.
- [8] X H Meng, M X Li, L X Wu, et al. Analysis and countermeasure of defects in welding automobile galvanized steel sheet. *Foundry Technology*, 2018, 39(3): 625–627.
- [9] W Chen, P Ackerson, P Molian. CO<sub>2</sub> laser welding of galvanized steel sheets using vent holes. *Materials & Design*, 2009, 30(2): 245–251.
- [10] W Reimann, S Pfriem, T Hammer, et al. Influence of different zinc coatings on laser brazing of galvanized steel. *Journal of Materials Processing Tech.*, 2017, 239: 75–82.
- [11] J Grajczak, S Nothdurft, J Hermsdorf. Investigations on pulsed laser beam welding of thin steel sheets in lap configuration over the face side/parallel joint. *Procedia CIRP*, 2020, 94: 680–685.
- [12] J Liu, H Zhang, Y Shi. Technology optimizing research on laser nonpenetration lap welding of stainless steel based on design-expert V7. *Journal of Mechanical Engineering*, 2011, 47(16): 9–13. (in Chinese)
- [13] X Z Guo, W Liu, J F Fan, et al. Welding residual stress and deformation of full and partial penetration laser welded lap joints. *Chinese Journal of Lasers*, 2020, 47(5): 353–361. (in Chinese)
- [14] R Wang, M J Ma, W L Chen. Welding technology, microstructure and mechanical properties of SUS301L stainless steel lap welded joint by cold metal transfer technology. *Electric Welding Machine*, 2017, 47(10): 53–57.
- [15] H Huang, J D Wang, L Q Li, et al. Prediction of laser welding induced deformation in thin sheets by efficient numerical modeling. *Journal of Materials Processing Technology*, 2016, 227: 117–128.
- [16] S Matsuoka, Y Okamoto, A Okada. Influence of weld bead geometry on thermal deformation in laser micro-welding. *Procedia CIRP*, 2013, 6: 492–497.
- [17] M S Choobi, M Haghpanahi, M Sedighi. Prediction of welding-induced angular distortions in thin butt-welded plates using artificial neural networks. *Computational Materials Science*, 2012, 62: 152–159.
- [18] J Liu. *Research on laser lap welding technology of SUS301L austenitic stainless steel for railway vehicles*. Changchun: Changchun University of Science and Technology, 2012. (in Chinese)
- [19] Y Liu, N S Ma, F G Lu, et al. Measurement and analysis of welding deformation in arc welded lap joints of thin steel sheets with different material properties. *Journal of Manufacturing Processes*, 2021, 61: 507–517.
- [20] E Z Liu. *Research of bulging distortion on the surface of unmelted side in thin plates partial penetration laser welding*. Shanghai: Shanghai Jiao Tong University, 2020. (in Chinese)
- [21] E Z Liu, C W Yao, Y L Xie, et al. Deformation mechanism of SUS304 austenitic stainless steel at weldless side in partial penetration laser welding. *Chinese Journal of Lasers*, 2019, 46(4): 49–57. (in Chinese)
- [22] A Ahola, T Bjork, Z Barsoum. Fatigue strength capacity of load-carrying fillet welds on ultra-high-strength steel plates subjected to out-of-plane bending. *Engineering Structures*, 2019, 196(Oct.1): 109282.1–109282.11.
- [23] Y Sun, A He, Y T Liang, et al. In-plane bending behaviour and capacities of S690 high strength steel welded I-section beams. *Journal of Constructional Steel Research*, 2019, 162(Nov.): 105741.1–105741.13.
- [24] J H An, S P Hong, Y J Kim, et al. Elastic stresses for 90° elbows under in-plane bending. *International Journal of Mechanical Sciences*, 2011, 53(9): 762–776.
- [25] Y H Yang, S Liu, J G Li, et al. Inhibitory effect of Ni-P coating on thermal expansion of carbon steel. *Surface & Coatings Technology*, 2017: 315484–489.
- [26] J X Fu, X D Li, W S Hwang. Study of the coefficient of thermal expansion for steel Q235. *Advanced Engineering Materials: Trans. Tech. Publications*, 2011: 324–328.
- [27] Y Ozturk, I Akkaya, E B Cevizci. A simple interferometric configuration for measurement of the coefficient of thermal expansion of selected metals. *Lasers in Engineering*, 2018, 41(1/3): 101–110.
- [28] J C Simmons, X B Chen, A Azizi, et al. Influence of processing and microstructure on the local and bulk thermal conductivity of selective laser melted 316L stainless steel. *Additive Manufacturing*, 2020, 32: 1–4.
- [29] R S Graves, T G Kollie, D L McElroy, et al. The thermal conductivity of AISI 304L stainless steel. *International Journal of Thermophysics*, 1991, 12(2): 409–415.
- [30] S Fan, R Ding, J Zheng, et al. Refined model for the stress-strain curve of austenitic stainless-steel materials at elevated temperatures. *Journal of Materials in Civil Engineering*, 2020, 32(4): 04020032.1–04020032.15.
- [31] N Masashi, F Yuya, O Mie. High temperature mechanical properties of harmonic structure designed SUS304L austenitic stainless steel. *Materials Science Forum*, 2017, 879(Pt.3): 2507–2511.